JOURNAL OF SOLID STATE CHEMISTRY **139,** 185–193 (1998)
ARTICLE NO. SC987831

Synthesis and Structural Evolution of the Solid Solution $Bi(Bi_{12-x}Te_xO_{14})Mo_{4-x}V_{1+x}O_{20}$ ($0 \leq x < 2.5$)

A. Castro,*,† R. Enjalbert,*,[1] P. Baules,* and J. Galy*

*Centre d'Elaboration de Matériaux et d'Etudes Structurales, CNRS, 29 rue Jeanne Marvig, B.P. 4347, 31055 Toulouse Cedex 4, France; and †Instituto de Ciencia de Materiales de Madrid, CSIC, Cantoblanco, 28049 Madrid, Spain

Received October 29, 1997; in revised form March 18, 1998; accepted March 20, 1998

A new solid solution of general formula $Bi(Bi_{12-x}Te_xO_{14})Mo_{4-x}V_{1+x}O_{20}$ with x up to 2.5 has been prepared by simultaneous substitution of the couple Te^{4+}–V^{5+} for Bi^{3+}–Mo^{6+} in $Bi_{13}Mo_4VO_{34}$. These materials have been studied by X-ray powder diffraction and thermal analysis, showing a structural evolution with changing x values. Crystal growth of these phases has been carried out; the single crystals have been studied by transmission electron microscopy and their structure determined by X-ray single crystal diffraction techniques performed for the $x = 1$ and $x = 2$ samples. Both materials crystallize in a monoclinic unit cell, space groups $P2$ for $Bi(Bi_{11}TeO_{14})Mo_3V_2O_{20}$ ($x = 1$) and $P2/c$ for $Bi(Bi_{10}Te_2O_{14})Mo_2V_3O_{20}$ ($x = 2$), with respective unit-cell parameters $a = 11.704(9)$, $b = 5.820(1)$, $c = 12.16(1)$ Å, $\beta = 100.90(2)^\circ$ ($Z = 1$) and $a = 11.642(2)$, $b = 5.771(1)$, $c = 24.22(1)$ Å, $\beta = 101.16(4)^\circ$ ($Z = 2$). The structures keep the basic framework of "columns" present in the parent oxide $Bi(Bi_{12}O_{14})Mo_4VO_{20}$; they are built up by infinite $(Bi_{12-x}Te_xO_{14})$ columns along the [010] direction and surrounded by independent $(Mo, V)O_4$ tetrahedra organized in layers parallel to (100) and (001) planes. The extra Bi cations are located at the intersection of these layers. The $x = 1$ compound exhibits original structural features due to its acentric structure. The observed structural evolution can be correlated to the different charge balance between columns $(Bi_{12-x}Te_xO_{14})^{(8+x)+}$ and tetrahedral environment, as well as to the lower stereochemical activity of the $6s^2$ lone pair of electrons of Bi^{3+} relative to the $5s^2$ electrons of Te^{4+} cation. © 1998 Academic Press

INTRODUCTION

Various compounds belonging to the phase diagram of the Bi_2O_3–MoO_3 system have been widely studied (1–5) because of their effective catalytic properties for selective oxidation and ammonoxidation of olefines (6–9). One of the most interesting oxides of this system is Bi_2MoO_6, which exhibits three polymorphic forms (10). The low temperature polymorph, γ(L), is the mineral keochlinite showing a layered Aurivillius-type structure with alternating $(Bi_2O_2)_n$ sheets and $(MoO_4)_n$ layers consisting of corner-shared distorted MoO_6 octahedra (11). On heating, γ(L) phase transforms reversibly at 570°C to an intermediate phase, γ(I), which has been reported as another layered structure (12). Finally, at 604°C the transition from γ(I) to the high temperature form, γ(H), occurs slowly and irreversibly. The structure of the high temperature polymorph of Bi_2MoO_6 has been determined from the refinement of high-resolution neutron powder diffraction data (13) and X-ray diffraction single crystal methods (14). In this structure the cation distribution forms a fluorite-related network with infinite channels of bismuth–oxygen polyhedra, surrounded by molybdenum–oxygen tetrahedra.

Several controversies and uncertainties have remained about the phases present in the bismuth-rich part of the Bi_2O_3–MoO_3 system, particularly with respect to the existence of a solid solution around 1.3 Bi_2O_3–MoO_3 composition and the structural characteristics of the $Bi_{26}Mo_{10}O_\delta$ phase (15, 16). This oxide was previously detected by Erman *et al.* (1), Miyazawa *et al.* (2), and Chen *et al.* (3). Recently, the true limits of that solid solution, as well as the accurate structure of the isostructural stoichiometric compound $Bi(Bi_{12}O_{14})Mo_4VO_{20}$ (17), have been reported. This oxide exhibits a structure related to γ(H)-Bi_2MoO_6 and can be described as built up by infinite $(Bi_{12}O_{14})_n$ columns surrounded by $(Mo, V)O_4$ tetrahedra and an extra isolated Bi atom located between two tetrahedra.

On the other hand, the possible substitution of M* cations possessing a stereoactive lone pair of electrons, such as Pb^{2+}, Sb^{3+}, Te^{4+} … for Bi^{3+} in Aurivillius-type structures (18–20)—for instance in Sb_2MoO_6 (21), which is similar to γ(L)-Bi_2MoO_6—and the influence of such substitution on electrical properties (22–24), have been widely studied. Moreover, the new $Pb(Bi_{12}O_{14})Mo_5O_{20}$ compound has been reported as isostructural to the "columns"-phases, the

[1]To whom correspondence should be addressed. Fax: (33) 05 62 25 79 99. E-mail: enjalber@cemes.fr.

0022-4596/98 $25.00

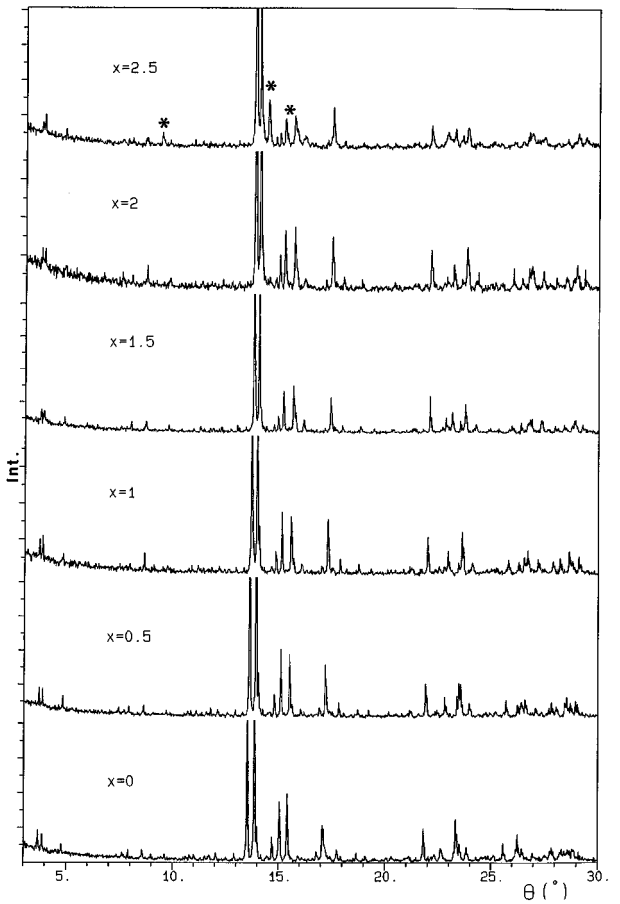

FIG. 1. X-ray diffraction patterns of $Bi(Bi_{12-x}Te_xO_{14})Mo_{4-x}V_{1+x}O_{20}$ phases (* is $BiVO_4$ oxide).

isolated cation position between tetrahedra being occupied by Pb^{2+} cations (25).

With the aim of improving the electrical properties of the "columns"-phases and understanding their complicated structural characteristics, obviously related to the lone pair's stereochemical activity (26), we have undertaken the synthesis of new materials belonging to this family by cationic substitution, changing the charge balance between columns and tetrahedral environment. Te^{4+} has been chosen to substitute the Bi^{3+} due to the similar stereochemical behavior of respectively, the Te^{4+} $5s^2$ and Bi^{3+} $6s^2$ lone pair of electrons. In order to compensate the greater charge of Te^{4+}, simultaneous doping by V^{5+} for Mo^{6+} has been carried out.

EXPERIMENTAL

Synthesis

Polycrystalline samples were prepared by solid state reaction from appropriate amounts of stoichiometric mixtures of analytical-grade Bi_2O_3, TeO_2, MoO_3, and V_2O_5. The reactants were thoroughly mixed in an agate mortar and processed in alumina crucibles in the temperature sequence: 500°C, 600°C for 24 h, and 600°C for 12 h. After each thermal treatment, the samples were quenched in air, weighed, reground, and examined by X-ray powder diffraction methods.

Single crystals of every composition were grown by two different methods: from melting of prepared powdered samples and by a flux method from stoichiometric mixtures of Bi_2O_3, MoO_3, and V_2O_5 in presence of an excess of TeO_2 acting as a flux. The growth protocol was the same for both

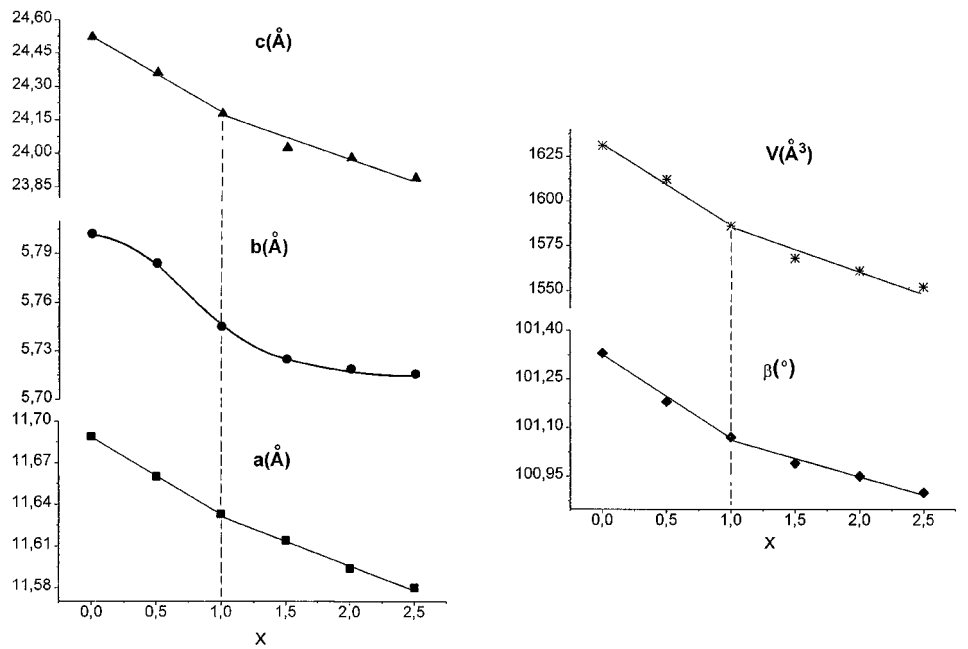

FIG. 2. Unit-cell parameters evolution (measured from X-ray powder diffraction data) for $Bi(Bi_{12-x}Te_xO_{14})Mo_{4-x}V_{1+x}O_{20}$ solid solution (powder synthesis at 600°C).

methods: starting products were placed into Pt crucibles and heated at 910°C for 4 h, then cooled to 400°C at $5°h^{-1}$ and to room temperature at $50°h^{-1}$. This protocol results in the formation of yellow parallelepiped crystals of adequate size to be studied by X-ray single crystal diffraction methods.

The compositions of single crystals were verified by chemical analysis (ICP atomic emission spectroscopy) and were found to be the same for both growth methods, in good agreement with the compositions of powdered samples used in the melting procedure.

Thermal Analysis

The differential scanning calorimetric curves (DSC) were obtained in static air atmosphere pressure and N_2 flow in the temperature range -100 to 600°C on a Seiko 220-CU DSC analyzer, at a heating-cooling rate of $10° \cdot min^{-1}$ and an initial weight of about 120 mg. Alumina was the reference material. Thermogravimetric curves were performed in the same conditions, between 25 and 650°C, on a Stanton Redcroft STA-781 instrument.

Structural Studies

Powder X-ray diffraction patterns were recorded using graphite monochromatized Cu$K\alpha$ radiation, with a Seifert XRD 3000 diffractometer, scanning from 2° to 32°(θ) by steps of 0.025°(θ) and counting rates of 3 s per step. Unit-cell parameters derived from X-ray powder data were calculated.

The single crystal quality and the crystal systems were first investigated using a precession camera. The diffraction data were collected using an Enraf-Nonius CAD4 diffractometer. Orientation matrix and cell parameters were obtained from least-squares refinements of setting angles of 25 reflections. Corrections of Lorentz-polarization and empirical absorption (27) were applied to *hkl* data. Atomic scattering factors were corrected for anomalous dispersion (28). The calculations were performed with SHELXL96 (29) and drawings with ORTEP (30).

Electron Microscopy

The three samples corresponding to $x = 0$, 1, and 2 were prepared from powder and deposited on a copper grid covered by a thin carbon layer. The electronic diffraction patterns were performed on a Philips CM20 in transmission mode working with an accelerating voltage of 200 KV.

RESULTS AND DISCUSSION

Six phases of nominal composition $Bi(Bi_{12-x}Te_xO_{14})Mo_{4-x}V_{1+x}O_{20}$ for $x = 0$, 0.5, 1, 1.5, 2, and 2.5 were prepared as very well crystallized microcrystalline powders. The well-characterized compound (17) $Bi(Bi_{12}O_{14})Mo_4VO_{20}$ phase was also prepared for comparative purposes. When both tellurium and vanadium contents were increased, the color of samples evolves from pale yellow for

TABLE 1
Lattice Parameters Refined on Single Crystals (Obtained at 910°C) for the Phases of $Bi(Bi_{12-x}Te_xO_{14})Mo_{4-x}V_{1+x}O_{20}$ Solid Solution

x	a (Å)	b (Å)	c (Å)	β (°)	V (Å^3)
0	11.652(7)	5.792(1)	24.42(1)	101.38(6)	1616(1)
0.5	11.656(3)	5.775(2)	24.28(2)	101.32(5)	1602(1)
1	11.704(9)	5.820(1)	12.16(1)	100.90(2)	813(1)
1.5	11.658(2)	5.777(1)	24.30(1)	101.15(4)	1606(1)
2	11.642(2)	5.771(1)	24.22(1)	101.16(4)	1597(1)

TABLE 2
Crystallographic Data for $x = 1$ and $x = 2$ Phases of $Bi(Bi_{12-x}Te_xO_{14})Mo_{4-x}V_{1+x}O_{20}$ Solid Solution

	$x = 1$	$x = 2$
	Crystal data	
Formula	$Bi_{12}TeMo_3V_2O_{34}$	$Bi_{11}Te_2Mo_2V_3O_{34}$
Crystal system	Monoclinic	Monoclinic
Space group	$P2$	$P2/c$
a (Å)	11.704(9)	11.642(2)
b (Å)	5.820(1)	5.771(1)
c (Å)	12.16(1)	24.22(1)
β (°)	100.90(2)	101.16(4)
V (Å)^3	813(1)	1597(1)
Z	1	2
Molecular weight	3569	3442
ρ calc ($g \cdot cm^{-3}$)	7.29	7.16
μ (Mo$K\alpha$) (cm^{-1})	673	639
Morphology	Parallelepiped	Parallelepiped
Color	Yellow	Yellow
Dimensions (mm)	$0.085 \times 0.115 \times 0.185$	$0.094 \times 0.138 \times 0.150$
	Data Collection	
Temperature (°C)	20	20
Wavelength (Mo$K\alpha$) (Å)	0.71069	0.71069
Monochromator	Graphite	Graphite
Scan mode	ω–2θ	ω–2θ
Scan width (°)	$0.80 + 0.35 \tan\theta$	$0.80 + 0.35 \tan\theta$
Take-off angle (°)	3.2	3.7
T_{max} (s)	60	60
Max Bragg angle (°)	35	32
hkl range	$-18 \rightarrow 18/0 \rightarrow 9/0 \rightarrow 19$	$-17 \rightarrow 16/0 \rightarrow 8/0 \rightarrow 35$
	Structure refinement	
Refinement of F^2		
Reflections measured/used	3542/2828	2768/2663
Parameters	150	151
$R[F^2 > 2\sigma(F)^2]$	0.080	0.082
Extinction coeff.	0.0004(2)	0.00017(6)
Flack coeff.	0.08(3)	none
S coeff.	1.03	1.04

$x = 0$ to deep yellow for $x = 2$; finally for $x = 2.5$, the product becomes orange.

Figure 1 shows the X-ray diffraction patterns of all the obtained compounds $Bi(Bi_{12-x}Te_xO_{14})Mo_{4-x}V_{1+x}O_{20}$. Significant displacements in the diffraction lines are observed. For $0 \leq x \leq 2$, the "columns" single phase appears to be present, while the $x = 2.5$ sample contains primarily the "columns"-phase but mixed with a small amount of $BiVO_4$ oxide. Unit-cell constants have been determined from the powder diffraction patterns. For the sake of clarity the c and V parameters of the phase corresponding to $x = 1$ have been doubled to follow the evolution with x (Fig. 2). It shows a continuous decrease of both a, b, c, β, and V parameters as a function of increasing Te^{4+} and V^{5+} concentration, including for the $x = 2.5$ phase. Significant slope changes occur around the $x = 1$ value. The most significant discontinuity occurs with respect to the b lattice parameter. This observation leads to the hypothesis that something particular happens in the structure at the $x = 1$ value, may be an order-disorder phenomenon due to preferential site occupancy or electric charge balance. The general lattice evolution can be reasonably related to the substitution of the smaller Te^{4+} and V^{5+} cations for the larger Bi^{3+} and Mo^{6+} respectively ($r_{Te^{4+}} = 0.66$ Å, $r_{Bi^{3+}} = 0.96$ Å, $r_{V^{5+}} = 0.355$ Å, $r_{Mo^{6+}} = 0.41$ Å) (31). Thus, it can be concluded that $Bi(Bi_{12-x}Te_xO_{14})Mo_{4-x}V_{1+x}O_{20}$ forms a solid solution

TABLE 3
Positional and Thermal Atomic Parameters for $x = 1$ and $x = 2$ Phases of $Bi(Bi_{12-x}Te_xO_{14})Mo_{4-x}V_{1+x}O_{20}$ Solid Solution

Atom	x	y	z	U_{eq} (Å^2)	Site occ.
		$x = 1$			
Bi/Te1	0.0350 (1)	0.40	0.6554 (1)	0.0156 (2)	0.92/0.08
Bi/Te2	0.1582 (1)	− 0.1021 (4)	0.4928 (1)	0.0173 (2)	0.92/0.08
Bi/Te3	0.2307 (1)	− 0.0042 (4)	0.8023 (1)	0.0188 (2)	0.92/0.08
Bi/Te4	0.3575 (1)	0.4841 (4)	0.6479 (1)	0.0180 (2)	0.92/0.08
Bi/Te5	0.2755 (1)	0.4887 (4)	0.3164 (1)	0.0190 (2)	0.92/0.08
Bi/Te6	− 0.0882 (1)	− 0.0137 (4)	0.8164 (1)	0.0181 (2)	0.92/0.08
Bi7	0.5109 (4)	0.4407 (5)	0.0109 (4)	0.0325 (9)	0.50
Mo/V1	1/2	− 0.006 (1)	1/2	0.0162 (7)	0.60/0.40
Mo/V2	0.1706 (3)	0.5187 (7)	− 0.0280 (2)	0.0138 (6)	0.60/0.40
Mo/V3	0.4264 (3)	− 0.0260 (9)	0.1532 (3)	0.0168 (7)	0.60/0.40
O1	0	0.230 (6)	1/2	0.011 (5)[a]	1
O2	0	0.716 (7)	1/2	0.014 (6)[a]	1
O3	0.221 (3)	0.267 (6)	0.671 (3)	0.023 (5)[a]	1
O4	0.235 (3)	0.749 (6)	0.674 (3)	0.023 (5)[a]	1
O5	0.264 (2)	0.586 (6)	0.488 (2)	0.027 (5)[a]	1
O6	0.142 (2)	0.744 (4)	0.313 (2)	0.011 (4)[a]	1
O7	0.140 (3)	0.258 (6)	0.314 (3)	0.022 (5)[a]	1
O8	0.053 (2)	0.045 (5)	0.716 (2)	0.022 (5)[a]	1
O9	0.367 (5)	0.18 (1)	0.493 (5)	0.07 (2)[a]	1
O10	0.481 (5)	− 0.20 (1)	0.378 (5)	0.08 (2)[a]	1
O11	0.375 (3)	0.045 (7)	0.019 (3)	0.037 (7)[a]	1
O12	0.314 (3)	− 0.001 (9)	0.221 (3)	0.039 (7)[a]	1
O13	0.526 (3)	0.685 (7)	0.858 (3)	0.038 (7)[a]	1
O14	0.458 (3)	0.164 (8)	0.801 (3)	0.040 (8)[a]	1
O15	0.189 (3)	0.548 (8)	0.115 (3)	0.040 (8)[a]	1
O16	0.309 (3)	0.541 (8)	− 0.078 (3)	0.041 (8)[a]	1
O17	0.084 (4)	0.736 (9)	− 0.091 (4)	0.044 (9)[a]	1
O18	0.102 (5)	0.28 (1)	− 0.072 (5)	0.07 (2)[a]	1

Atom	U_{11}	U_{22}	U_{33}	U_{23}	U_{13}	U_{12}
Bi/Te1	0.0151 (5)	0.0198 (5)	0.0119 (4)	− 0.0019 (5)	0.0029 (3)	− 0.0003 (5)
Bi/Te2	0.0154 (5)	0.0188 (5)	0.0178 (5)	0.0009 (6)	0.0033 (4)	− 0.0001 (5)
Bi/Te3	0.0189 (5)	0.0229 (6)	0.0134 (4)	− 0.0009 (6)	0.0002 (3)	0.0016 (6)
Bi/Te4	0.0117 (4)	0.0220 (5)	0.0196 (5)	0.0046 (6)	0.0012 (3)	− 0.0001 (6)
Bi/Te5	0.0127 (4)	0.0227 (5)	0.0229 (5)	− 0.0037 (6)	0.0064 (4)	− 0.0019 (6)
Bi/Te6	0.0210 (5)	0.0221 (5)	0.0119 (4)	− 0.0008 (6)	0.0046 (4)	− 0.0015 (6)
Mo/V1	0.013 (2)	0.014 (2)	0.022 (2)	0	0.003 (1)	0
Mo/V2	0.015 (1)	0.019 (2)	0.007 (1)	0.001 (1)	0.0009 (8)	0.001 (1)
Mo/V3	0.009 (1)	0.025 (2)	0.017 (1)	− 0.001 (1)	0.0014 (9)	− 0.002 (1)

TABLE 3—*Continued*

Atom	x	y	z	U_{eq} (Å^2)	Site occ.
		$x = 2$			
Bi/Te1	0.0379 (1)	0.4177 (3)	0.32788 (7)	0.0169 (3)	0.83/0.17
Bi/Te2	0.1587 (1)	− 0.0843 (3)	0.24495 (7)	0.0199 (3)	0.83/0.17
Bi/Te3	0.2357 (1)	0.0022 (4)	0.40233 (7)	0.0242 (3)	0.83/0.17
Bi/Te4	0.3591 (1)	0.4944 (4)	0.32079 (7)	0.0236 (3)	0.83/0.17
Bi/Te5	0.2731 (1)	0.4952 (4)	0.15643 (7)	0.0231 (3)	0.83/0.17
Bi/Te6	− 0.0820 (1)	0.0011 (4)	0.41184 (6)	0.0206 (3)	0.83/0.17
Bi7	0.5139 (5)	0.500 (2)	0.0058 (3)	0.045 (1)[a]	0.50
Mo/V1	1/2	0.006 (2)	1/4	0.023 (1)	0.40/0.20
Mo/V2	0.1697 (4)	0.510 (1)	0.4873 (2)	0.0204 (9)	0.40/0.20
Mo/V3	0.4262 (3)	− 0.007 (1)	0.0800 (2)	0.0204 (9)	0.40/0.20
O1	0	0.226 (9)	1/4	0.03 (1)[a]	1
O2	0	0.723 (7)	1/4	0.019 (8)[a]	1
O3	0.228 (3)	0.265 (5)	0.335 (1)	0.025 (6)[a]	1
O4	0.239 (3)	0.755 (5)	0.335 (1)	0.026 (6)[a]	1
O5	0.257 (3)	0.573 (7)	0.243 (2)	0.042 (8)[a]	1
O6	0.137 (2)	0.252 (5)	0.652 (1)	0.019 (5)[a]	1
O7	0.140 (3)	0.744 (6)	0.656 (1)	0.030 (7)[a]	1
O8	0.059 (2)	0.051 (5)	0.364 (1)	0.023 (6)[a]	1
O9	0.375 (4)	0.17 (1)	0.248 (2)	0.07 (1)[a]	1
O10	0.485 (7)	− 0.14 (2)	0.191 (3)	0.13 (3)[a]	1
O11	0.382 (6)	0.04 (1)	0.013 (3)	0.11 (2)[a]	1
O12	0.320 (4)	− 0.00 (1)	0.116 (2)	0.07 (1)[a]	1
O13	0.494 (4)	0.731 (9)	0.081 (2)	0.07 (1)[a]	1
O14	0.476 (8)	0.21 (2)	0.400 (4)	0.18 (4)[a]	1
O15	0.184 (5)	0.46 (1)	0.054 (3)	0.09 (2)[a]	1
O16	0.300 (4)	0.445 (9)	0.464 (2)	0.06 (1)[a]	1
O17	0.108 (3)	0.743 (8)	0.451 (2)	0.047 (9)[a]	1
O18	0.087 (5)	0.28 (1)	0.472 (3)	0.10 (2)[a]	1

Atom	U_{11}	U_{22}	U_{33}	U_{23}	U_{13}	U_{12}
Bi/Te1	0.0149 (6)	0.0166 (6)	0.0195 (7)	− 0.0020 (6)	0.0041 (5)	− 0.0012 (5)
Bi/Te2	0.0126 (6)	0.0166 (7)	0.0314 (8)	0.0002 (7)	0.0061 (5)	− 0.0010 (5)
Bi/Te3	0.0198 (7)	0.0232 (7)	0.0281 (8)	− 0.0023 (9)	0.0008 (5)	0.0036 (8)
Bi/Te4	0.0120 (6)	0.0212 (7)	0.0367 (8)	0.0046 (9)	0.0022 (5)	− 0.0014 (8)
Bi/Te5	0.0113 (6)	0.0228 (7)	0.0365 (8)	− 0.0049 (9)	0.0076 (5)	− 0.0036 (7)
Bi/Te6	0.0198 (7)	0.0216 (6)	0.0213 (7)	− 0.0001 (8)	0.0065 (5)	− 0.0041 (8)
Mo/V1	0.007 (2)	0.020 (3)	0.042 (4)	0	0.010 (2)	0
Mo/V2	0.028 (2)	0.020 (2)	0.012 (2)	0.000 (2)	0.003 (2)	0.002 (2)
Mo/V3	0.006 (2)	0.028 (2)	0.029 (2)	− 0.003 (2)	0.008 (1)	− 0.002 (2)

Note. $U_{eq.} = 1/3$ trace U.
[a] U_{iso}.

belonging to the "columns" structural type with the upper limit close to $x = 2.5$. This fact cannot be altered by variations in the reactions conditions.

In order to investigate the existence of possible phase transitions in the solid solution, both thermogravimetric and scanning calorimetric analysis have been performed. TG curves show that all phases are stable in the whole range of temperature studied, from room temperature up to 625°C without any weight loss for each x value.

On the other hand, on heating DSC curves only reveal the appearance of an irreversible endothermic peak centered at

TABLE 4
Bond Distances (Å) for $Bi(Bi_{12-x}Te_xO_{14})Mo_{4-x}V_{1+x}O_{20}$ $x = 1$ and $x = 2$ Phases

$x = 1$		$x = 2$	
Bi/Tel O1	2.10(2)	Bi/Tel O1	2.16(3)
Bi/Tel O8	2.19(3)	Bi/Tel O8	2.29(3)
Bi/Tel O3	2.29(3)	Bi/Tel O3	2.36(3)
Bi/Tel O7a1	2.30(3)	Bi/Tel O7a2	2.37(3)
Bi/Te2 O2b1	2.15(2)	Bi/Te2 O2b2	2.18(2)
Bi/Te2 O5b1	2.20(3)	Bi/Te2 O5b2	2.29(4)
Bi/Te2 O6b1	2.33(2)	Bi/Te2 O4b2	2.40(3)
Bi/Te2 O4b1	2.37(3)	Bi/Te2 O6c2	2.42(3)
Bi/Te3 O4b1	2.13(3)	Bi/Te3 O8	2.10(3)
Bi/Te3 O8	2.17(2)	Bi/Te3 O4b2	2.16(3)
Bi/Te3 O3	2.24(3)	Bi/Te3 O3	2.22(3)
Bi/Te4 O3	2.09(3)	Bi/Te4 O5	2.07(4)
Bi/Te4 O5	2.13(3)	Bi/Te4 O3	2.10(3)
Bi/Te4 O4	2.17(3)	Bi/Te4 O4	2.13(3)
Bi/Te5 O7	2.07(3)	Bi/Te5 O7d2	2.07(3)
Bi/Te5 O6	2.15(2)	Bi/Te5 O6d2	2.14(3)
Bi/Te5 O5	2.19(3)	Bi/Te5 O5	2.20(4)
Bi/Te6 O6c1	2.12(2)	Bi/Te6 O6e2	2.14(3)
Bi/Te6 O7a1	2.24(3)	Bi/Te6 O8	2.20(3)
Bi/Te6 O8	2.26(2)	Bi/Te6 O7a2	2.22(3)
Bi7 O16d1	2.20(4)	Bi7 O16f2	2.17(5)
Bi7 O13el	2.24(4)	Bi7 O13	2.30(5)
Bi7 O13f1	2.37(4)	Bi7 O13g2	2.47(5)
Bi7 O16	2.48(4)	Bi7 O16d2	2.52(5)
Mo/V1 O10e1	1.84(7)	Mo/V1 O10	1.64(9)
Mo/V1 O10	1.84(7)	Mo/V1 O10f2	1.64(9)
Mo/V1 O9	1.87(6)	Mo/V1 O9f2	1.74(5)
Mo/V1 O9e1	1.87(6)	Mo/V1 O9	1.74(5)
Mo/V2 O18	1.66(7)	Mo/V2 O15h2	1.60(6)
Mo/V2 O17	1.71(5)	Mo/V2 O18	1.64(7)
Mo/V2 O15	1.72(3)	Mo/V2 O17	1.69(4)
Mo/V2 O16	1.84(3)	Mo/V2 O16	1.75(5)
Mo/V3 O11	1.69(3)	Mo/V3 O11	1.63(7)
Mo/V3 O12	1.69(3)	Mo/V3 O12	1.65(5)
Mo/V3 O14e1	1.76(4)	Mo/V3 O14f2	1.68(11)
Mo/V3 O13g1	1.78(4)	Mo/V3 O13b2	1.70(5)

Symmetry code:	Symmetry code:
a1 : $-x, y, -z+1$	a2 : $-x, -y+1, -z+1$
b1 : $x, y-1, z$	b2 : $x, y-1, z$
c1 : $-x, y-1, z+1$	c2 : $x, -y, z-1/2$
d1 : $-x+1, y, z$	d2 : $x, -y+1, z-1/2$
e1 : $-x+1, y, z+1$	e2 : $-x, -y, -z+1$
f1 : $x, y, z-1$	f2 : $-x+1, y, -z+1/2$
g1 : $-x+1, y-1, z+1$	g2 : $-x+1, -y+1, -z$
	h2 : $x, -y+1, z+1/2$

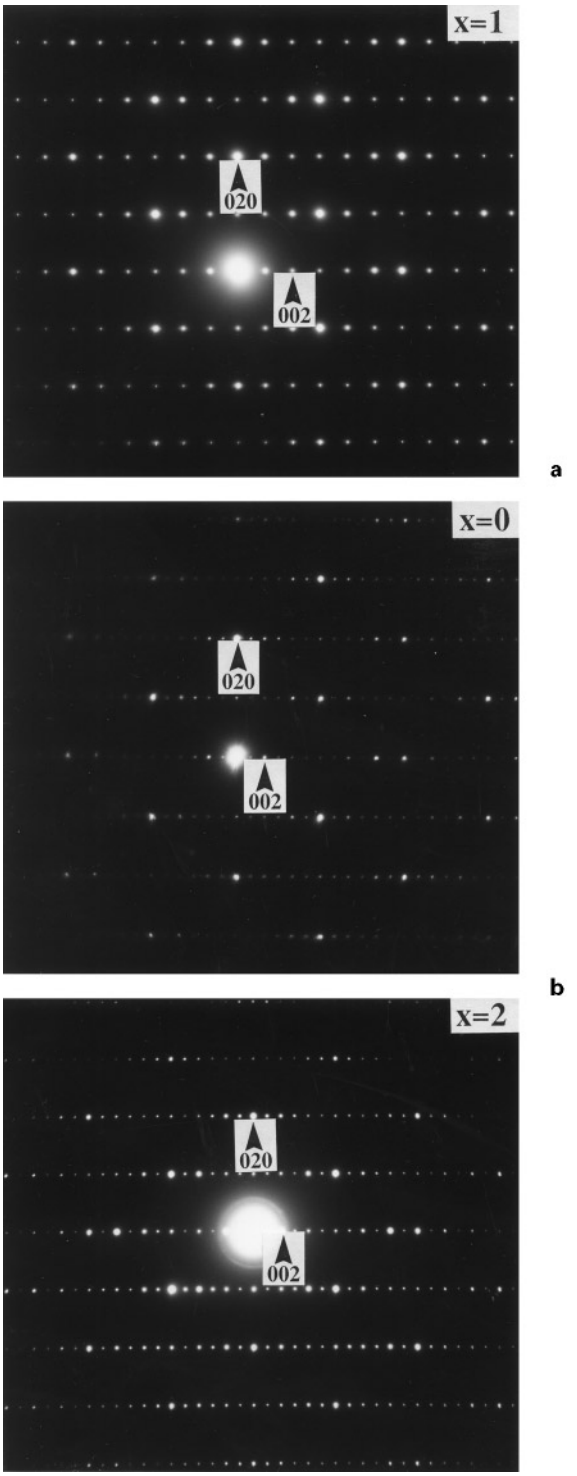

FIG. 3. (b^*, c^*) TEM diffraction patterns of $Bi(Bi_{12-x}Te_xO_{14})Mo_{4-x}V_{1+x}O_{20}$ phases: (a) $x = 1$ and (b) $x = 0$ and 2.

473, 415, and 489°C, with ΔH values of 0.72, 0.07, and $0.27\,J\cdot g^{-1}$, for $x = 0$, 1, and 2 phases respectively. This result can be compared with the DSC measurements reported by Vannier *et al.* (15), carried out on the less well-defined composition $Bi_{26}Mo_{10}O_{\delta}$. Those authors point out the existence of a reversible endothermic thermal effect at about 310°C, on heating, which they believe to be due to a transition between two polymorphic phases: triclinic at room temperature and monoclinic at high temperature. Their results seem to be corroborated by previous conductivity measurements, where the Arrhenius plot of $Bi_{26}Mo_{10}O_{\delta}$ shows a slope change at about 300°C, although such a transition is not observed for the "$Bi_{26}Mo_8V_2$" phase, which is quite similar to our $x = 0$ compound.

In fact, the thermal effects observed here for $x = 0$, 1, and 2 of $Bi(Bi_{12-x}Te_xO_{14})Mo_{4-x}V_{1+x}O_{20}$ phases cannot be correlated with a topological change within the structure, because the X-ray diffraction patterns before and after thermal treatments appear identical. We believe this might be due to an order-disorder transition like in γ-BIMEVOX oxides (32). Further studies are needed to establish the relation between structure and electrical properties of this solid solution. In this way, accurate high-temperature X-ray diffraction experiments together with impedance measurements are now in progress.

Since the intriguing evolution of the lattice parameters was seen by X-ray powder diffraction of the $Bi(Bi_{12-x}Te_xO_{14})Mo_{4-x}V_{1+x}O_{20}$ solid solution, we thought that the substitution of Te^{4+} for Bi^{3+} in the "columns" structure might lead to some exciting changes. Thus, we have grown single crystals for $x = 0$, 0.5, 1.0, 1.5, and 2.0 phases and undertaken their structural study by X-ray single crystal techniques.

Table 1 reports the unit-cell parameters refined on single crystal phases. As can be seen, a decrease of unit-cell volume is observed with increasing x value; as expected from the powdered samples, there is a discontinuity at $x = 1$. A peculiar behavior is exhibited by $Bi(Bi_{11}TeO_{14})Mo_3V_2O_{20}$ compound ($x = 1$) in that the c parameter is half of the ones in the remaining components of the solid solution. This interrupts the regular expected evolution of lattice constants. In order to understand the structural changes, the structures of

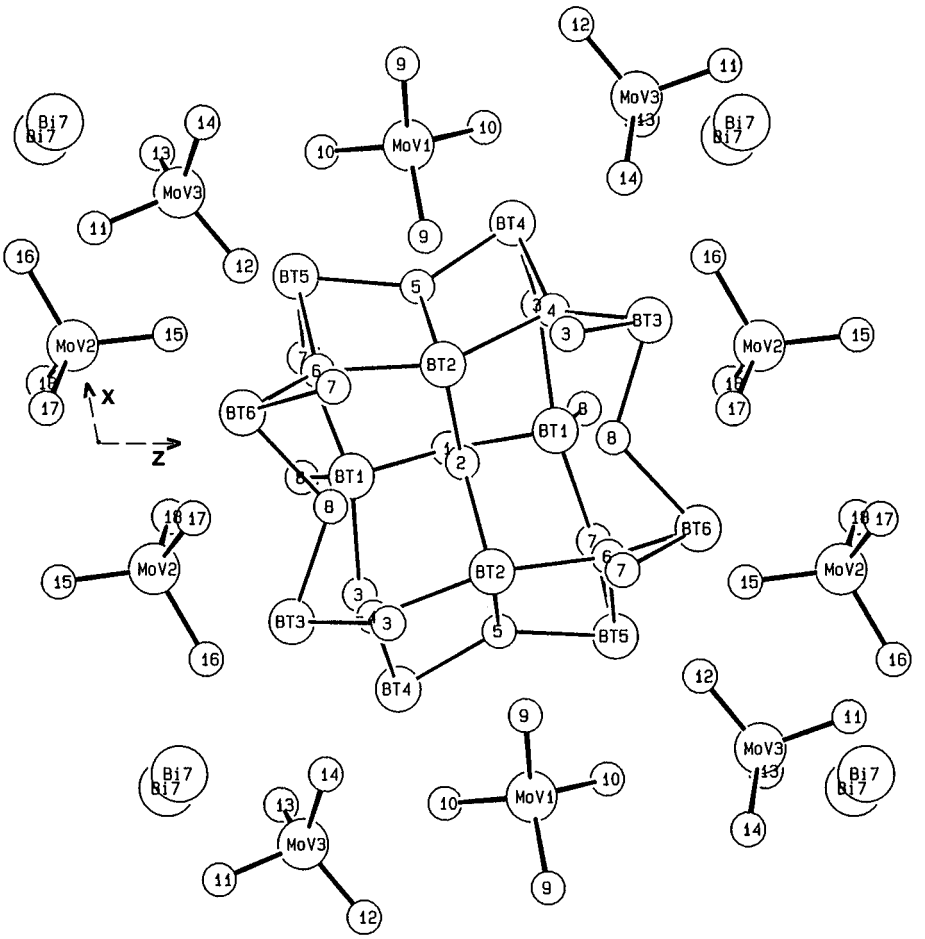

FIG. 4. View of $Bi(Bi_{11}Te_1O_{14})Mo_3V_2O_{20}$ structure.

the $Bi(Bi_{11}TeO_{14})Mo_3V_2O_{20}$, $x = 1$, and $Bi(Bi_{10}Te_2O_{14})Mo_2V_3O_{20}$, $x = 2$, oxides have been determined.

While the $x = 2$ compound retains the symmetry and space group $P2/c$ (No. 13) of the parent $Bi(Bi_{12}O_{14})Mo_4VO_{20}$ compound, the $x = 1$ phase crystallizes in a monoclinic unit cell but with an acentric space group ($P2$ (No. 3)). Table 2 summarizes physical and crystallographic data together with the conditions of data collection for both $x = 1$ and $x = 2$ phases. The very large absorption coefficients, which make accurate absorption corrections difficult, are responsible for the relatively high R value. The final positional and equivalent isotropic thermal parameters are listed in Table 3. Table 4 lists the main bond distances.

To complement the X-ray studies, phases corresponding to $x = 0$, 1, and 2 were studied by transmission electron microscopy. The (b^*, c^*) lattice planes obtained for each compound are shown in Fig. 3. The b parameter is similar for $x = 0$, 1, and $x = 2$. For $x = 1$, the c parameter is roughly half of the two others.

In both cases the general framework keeps the structural arrangement of the $Bi(Bi_{12}O_{14})Mo_4VO_{20}$, $x = 0$, parent compound (i.e., $Bi_{13}Mo_4VO_{34}E_{13}$, E = lone pair of electrons) (17). These phases are built up by infinite (Bi, Te)–O columns along the [010] direction, surrounded by $(Mo, V)O_4$ tetrahedra in layers parallel to (100) and (001) planes and isolated Bi atoms located at the intersection of those layers (see Figs. 2 and 3 of Ref. (17)). Interesting structural differences have been found in $x = 0$, 2, and 1 compounds, which will be explained below. The small dopant amounts would not facilitate any systematic ordering of the Mo/V and Bi/Te cations that could be directly observed. The cations were therefore statistically distributed in the corresponding positions. Figure 4 depicts the view for $x = 1$ phase of one column surrounded by 10 tetrahedra and Bi extra atoms. The atom labeling is the same for all the structures described. The refinement does not provide information about the location of Te atoms, except that they cannot be placed in the isolated Bi position, Bi7, due to its anomalous thermal parameter value and the divergence occurring in the refinement process.

Since the $x = 1$ and $x = 2$ compounds can be described in a very similar way as $Bi(Bi_{12}O_{14})Mo_4VO_{20}$, it is worthwhile to point out some original features observed. For both $x = 0$, 1 and 2 phases, the columns ($Bi_{12-x}Te_xO_{14}E_{12}$) are built up by an oxygen array around a skeleton of $(Bi, Te)_6$ octahedra sharing edges in planes quasiperpendicular to b, rotated 90° from level to level, and interconnected along the [010] direction. The angle between the basal planes of each pair of octahedra evolves from 14.6° to 16.6°. These planes fold up and down the perpendicular plane to b, in adjacent columns ($Bi_{12}O_{14}E_{12}$) and ($Bi_{10}Te_2O_{14}E_{12}$) in [001] direction for $x = 0$ and 2, due to the presence of the symmetry center. In $x = 1$ structure all ($Bi_{11}TeO_{14}E_{12}$) columns are oriented in the same direction (Fig. 5). In the same way, all the $(Mo, V)O_4$ tetrahedra are tilted away from the equilibrium found in the $x = 0$ parent structure, as can be seen in Fig. 6, as well as by the evolution of distances between oxygens belonging to tetrahedra, from O9 to O18, and bismuths or bismuths/telluriums outside the columns, from BT3 to BT6, reported in Table 5.

All the structural differences can be explained on the basis of electrostatic considerations. In fact, the electrical balance of charges between columns and surrounding tetrahedra evolves from $x = 0$ to $x = 2$. While for $Bi(Bi_{12}O_{14})Mo_4VO_{20}$ the columns are $(Bi_{12}O_{14})_n^{8n+}$ charged and the tetrahedra $(Mo_{4/5}V_{1/5}O_4)^{2.2-}$, for tellurium-doped phases the charge of columns increases up to $(Bi_{10}Te_2O_{14})_n^{10n+}$ and the tetrahedra to $(Mo_{2/5}V_{3/5}O_4)^{2.6-}$ for $x = 2$, thus giving rise to higher electrostatic interactions between "tetrahedra" and "columns" networks. On the other hand, the stereochemical activity of $5s^2$ lone pair of electrons of Te^{4+} and $6s^2$ of Bi^{3+} differs, allowing for higher repulsions between

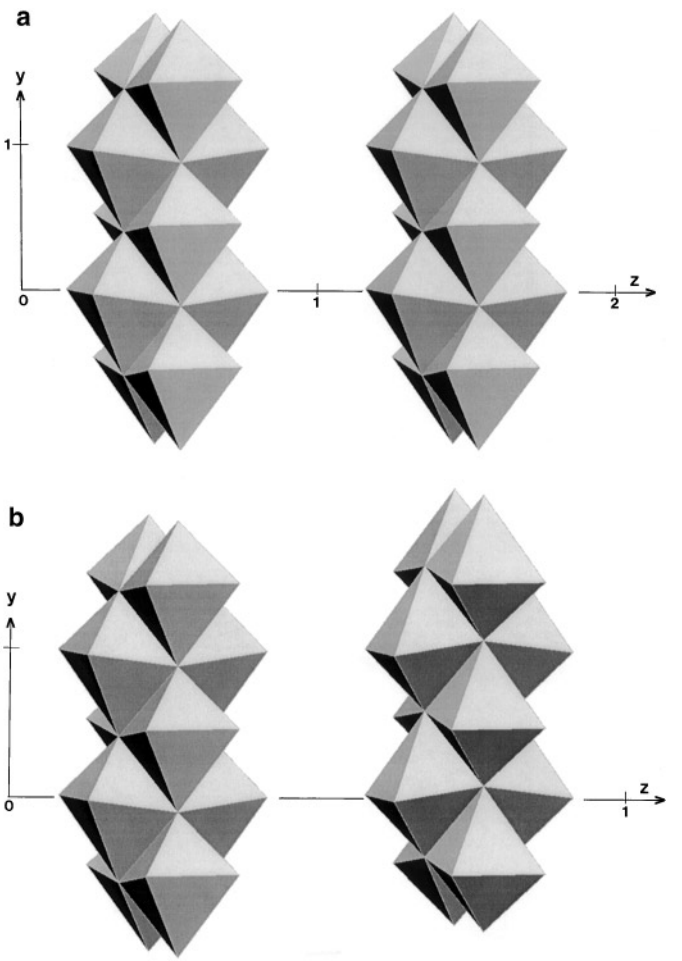

FIG. 5. Tilting of $(Bi, Te)_6$ octahedra in two adjacent ($Bi_{12-x}Te_xO_{14}$) columns of $Bi(Bi_{12-x}Te_xO_{14})Mo_{4-x}V_{1+x}O_{20}$ structures: (a) $x = 1$ and (b) $x = 2$.

oxygens and lone pairs (26) in the order $5s^2$ – oxygens $> 6s^2$ – oxygens.

Taking into account both small tellurium doping and important structural influences explained above, the electrical behavior of these materials must change such that the conduction is more pronounced in the tetrahedral layer between columns in the (100) plane or within columns, particularly for the more ordered $x = 1$ structure, i.e., the structure with $(Bi, Te)_6$ octahedra tilted in the same direction. The electrical properties of these materials are being studied for the various x values on single crystals and ceramic materials, and the results will be reported elsewhere.

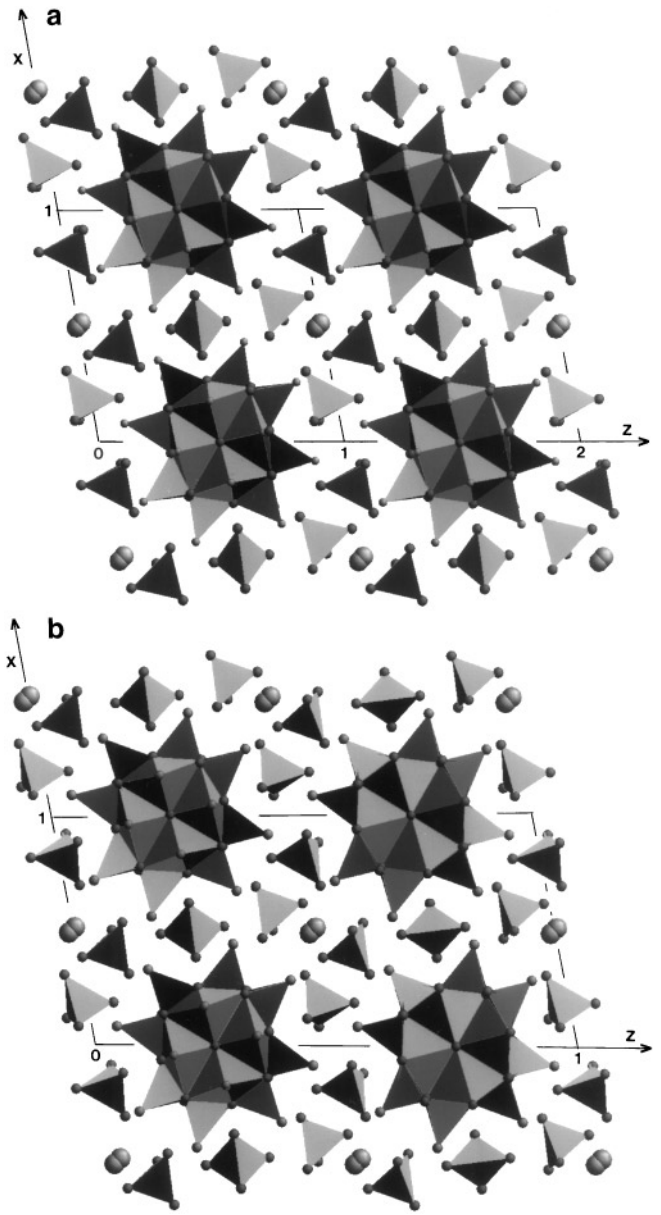

FIG. 6. Comparison between the projections onto the (010) plane of the crystal structures of $Bi(Bi_{12-x}Te_xO_{14})Mo_{4-x}V_{1+x}O_{20}$: (a) $x = 1$ and (b) $x = 2$.

TABLE 5

Selected Distances (Å) between O9–O18 Tetrahedral Oxygens and BT3–BT6 Column Cations for $x = 0$, 1, and 2 Phases of $Bi(Bi_{12-x}Te_xO_{14})Mo_{4-x}V_{1+x}O_{20}$ Solid Solution

$x = 0$			$x = 1$			$x = 2$		
Bi3	O17b2	2.50(6)	BT3	O17j1	2.78(3)	BT3	O17b2	2.55(3)
Bi3	O14	2.89(8)	BT3	O14	2.84(2)	BT3	O14	3.04(5)
Bi3	O16	3.15(5)	BT3	O16j1	3.07(3)	BT3	O16	2.98(4)
Bi3	O18	3.17(8)	BT3	O18h1	2.85(3)	BT3	O18	3.08(5)
Bi3	O13l2	3.47(7)	BT3	O13b1	3.85(2)	BT3	O13l2	3.47(5)
Bi4	O9	2.64(5)	BT4	O9	2.62(3)	BT4	O9	2.58(5)
Bi4	O14	2.67(7)	BT4	O14	2.73(3)	BT4	O14	2.71(5)
Bi4	O10m2	2.74(9)	BT4	O10k1	2.70(3)	BT4	O10m2	2.83(3)
Bi4	O13f2	2.86(6)	BT4	O13	3.15(2)	BT4	O13f2	2.98(3)
Bi4	O16	3.71(6)	BT4	O16h1	3.50(3)	BT4	O16	3.69(4)
Bi5	O15	2.50(7)	BT5	O15	2.49(2)	BT5	O15	2.50(5)
Bi5	O9	2.92(5)	BT5	O9	2.87(3)	BT5	O9	2.96(5)
Bi5	O10j2	3.13(9)	BT5	O10i1	2.99(3)	BT5	O10j2	3.22(3)
Bi5	O12j2	3.14(5)	BT5	O12i1	3.25(4)	BT5	O12j2	3.13(3)
Bi5	O13	3.71(7)	BT5	O13l1	3.62(3)	BT5	O13	3.70(4)
Bi6	O12i2	2.62(5)	BT6	O12a1	2.60(2)	BT6	O12i2	2.72(5)
Bi6	O18	2.73(6)	BT6	O18h1	2.91(3)	BT6	O18	2.73(3)
Bi6	O17b2	2.74(5)	BT6	O17j1	2.57(3)	BT6	O17b2	2.69(3)
Bi6	O15i2	3.04(7)	BT6	O15ml	3.00(3)	BT6	O15i2	3.10(3)
Bi6	O18e2	3.26(8)	BT6	O18a1	3.57(3)	BT6	O18e2	3.27(4)

Symmetry code:

a1 : $-x, y, -z+1$;	b1 : $x, y-1, z$;
c1 : $-x, y-1, z+1$;	d1 : $-x+1, y, z$;
e1 : $-x+1, y, z+1$;	f1 : $x, y, z-1$;
g1 : $-x+1, y-1, z+1$;	h1: $x, y, z+1$;
i1 : $x, y+1, z$;	j1 : $x, y-1, z+1$;
k1 : $-x+1, y+1, -z+1$;	l1 : $-x+1, y, -z+1$;
m1 : $-x+1, y-1, -z+1$	
a2 : $-x, -y+1, -z+1$;	b2 : $x, y-1, z$;
c2 : $x, -y, z-1/2$;	d2 : $x, -y+1, z-1/2$
e2 : $-x, -y, -z+1$;	f2 : $-x+1, y, -z+1/2$;
g2 : $-x+1, -y+1, -z$;	h2 : $x, -y+1, z+1/2$
i2: $-x, y, -z+1/2$;	j2 : $x, y+1, z$;
k2 : $x, -y, -z+1/2$;	l2 : $-x+1, y-1, -z+1/2$
m2: $-x+1, y+1, -z+1/2$;	n2 : $-x, y-1, -z+1/2$

Note. BT = Bi/Te

ACKNOWLEDGMENTS

A.C. thanks DGES and CICYT of Spain for financial support (Project MAT97-0711). She also expresses gratitude to CEMES/CNRS of France for their kind welcome.

REFERENCES

1. L. Y. Erman, E. L. Galpérin, and B. P. Soboler, *Russ. J. Inorg. Chem.* (*Engl. Transl.*) **16,** 258 (1971).
2. S. Miyazawa, A. Kawana, and H. Koizumi, *Mater. Res. Bull.* **9,** 41 (1974).
3. T. Chen and S. Smith, *J. Solid State Chem.* **10,** 288 (1975).

4. D. J. Buttrey, D. A. Jefferson, and J. M. Thomas, *Mater. Res. Bull.* **21,** 739 (1985).
5. L. E. Depero and L. Sangaleti, *J. Solid State Chem.* **119,** 428 (1995).
6. R. K. Grasselli and J. F. Burrington, *Adv. Catal.* **30,** 133 (1981).
7. R. K. Grasselli, *J. Chem. Educ.* **63,** 216 (1986).
8. D. J. Hucknall, "Selective Oxidation of Hydrocarbons." Academic Press, New York, 1974.
9. Ph. A. Batist, A. H. W. M. der Kinderen, Y. Leeuwenburgh, F. A. M. G. Metz, and G. C. A. Schuit, *J. Catal.* **12,** 45 (1968).
10. H. Kodama and A. Watanabe, *J. Solid State Chem.* **56,** 225 (1985).
11. K. S. Knight, *Miner. Magazine* **56,** 399 (1992).
12. L. Y. Erman and E. L. Galpérin, *Russ. J. Inorg. Chem.* (*Engl. Transl.*) **13,** 487 (1968).
13. D. J. Buttrey, T. Vogt, U. Wildgruber, and W. R. Robinson, *J. Solid State Chem.* **111,** 118 (1994).
14. R. Enjalbert, G. Hasselmann, and J. Galy, *in* "Proceedings of the Journées de la Division Chimie du Solide," Abstract no. A24, 1996.
15. R. N. Vannier, G. Mairesse, F. Abraham, and G. Nowogrocki, *J. Solid State Chem.* **122,** 394 (1996).
16. D. J. Buttrey, T. Vogt, G. P. A. Yap, and A. L. Rheingold, *Mater. Res. Bull.* **32,** 947 (1997).
17. R. Enjalbert, G. Hassselmann, and J. Galy, *J. Solid State Chem.* **131,** 236 (1997).
18. A. Castro, P. Millán, R. Enjalbert, E. Snöeck, and J. Galy, *Mater. Res. Bull.* **29,** 871 (1994).
19. A. Castro, P. Millán, M. J. Martínez-Lope, and J. B. Torrance, *Solid State Ionics* **63–65,** 897 (1993).
20. A. Ramírez, P. Millán, A. Castro, and J. B. Torrance, *Eur. J. Solid State Inorg. Chem.* **31,** 173 (1994).
21. A. Castro, R. Enjalbert, and J. Galy, *Acta Crystallogr. Sect. C* **53,** 1526 (1997).
22. A. Castro, P. Millán, B. Jiménez, R. Sirera, R. Jiménez, and J. B. Torrance, *Ferroelectrics* **153,** 255 (1994).
23. B. Jiménez, P. Durán-Martín, A. Castro, and P. Millán, *Ferroelectrics* **186,** 93 (1996).
24. A. Ramírez, R. Enjalbert, J. M. Rojo, and A. Castro, *J. Solid State Chem.* **128,** 30 (1997).
25. R. Enjalbert, G. Hasselmann, and J. Galy, *Acta Crystallogr. Sect. C* **53,** 269 (1997).
26. J. Galy, G. Meunier, S. Andersson, and A. Åström, *J. Solid State Chem.* **13,** 142 (1975).
27. A. C. T. North, D. C. Phillips, and F. S. Mattews, *Acta Crystallogr. Sect. A* **24,** 351 (1968).
28. D. T. Cromer and D. Liberman, "International Tables of X-Ray Crystallography," Vol IV. Kynoch Press, Birmingham, UK, 1974.
29. G. M. Sheldrick, "Program for the refinement of crystal structures." University of Göttingen, Germany, 1996.
30. C. K. Jonhson, "Ortep II Report ORNL 5138." Oak Ridge National Laboratory, Oak Ridge, TN, 1976.
31. R. D. Shannon, *Acta Crystallogr. Sect. A* **32,** 751 (1976).
32. E. Pernot, M. Anne, M. Bacmann, P. Strobel, J. Fouletier, R. N. Vannier, G. Mairesse, F. Abraham, and G. Nowogrocki, *Solid State Ionics* **70–71,** 259 (1994).